J. Phys.: Condens. Matter **23** (2011) 505101 (10pp) doi:10.1088/0953-8984/23/50/505101

Direct visualization of pH-dependent evolution of structure and dynamics in microgel suspensions

M Muluneh[1], J Sprakel[1,4], H M Wyss[2], J Mattsson[3] and D A Weitz[1]

[1] Department of Physics and School of Engineering and Applied Sciences, Harvard University, Cambridge, MA 02138, USA
[2] Mechanical Engineering and ICMS, Eindhoven University of Technology, 5600 MB Eindhoven, The Netherlands
[3] School of Physics and Astronomy, University of Leeds, Leeds LS2 9JT, UK

E-mail: mmuluneh@fas.harvard.edu

Received 25 August 2011, in final form 6 October 2011
Published 31 October 2011
Online at stacks.iop.org/JPhysCM/23/505101

Abstract
We use 3D confocal microscopy combined with image analysis and particle tracking techniques to study the structure and dynamics of aqueous suspensions of fluorescently labelled p(NIPAm-co-AAc) microgel particles. By adjusting the pH we can tune the interactions between the microgel particles from purely repulsive near neutral pH, to weakly attractive at low pH. This change in the interaction potential has a pronounced effect on the manner in which the suspensions solidify. We directly follow the evolution of the system after a quench from the liquid state to obtain detailed information on the route to kinetic arrest. At low pH and low concentration, dynamic arrest results mainly from crystallization driven by the attraction between particles; crystal nucleation occurs homogeneously throughout the sample and does not appear to be localized to geometric boundaries. Moreover, the growth of crystals is characterized by nucleation-limited kinetics where a rapid growth of crystal domains takes place after a long concentration-dependent lag time. At low pH and high concentration, relaxation of the suspension is constrained and it evolves only slightly, resulting in a disordered solid. At neutral pH, the dynamics are a function of the particle number concentration only; a high concentration leads to the formation of a disordered soft glassy solid.

(Some figures may appear in colour only in the online journal)

1. Introduction

Colloids serve as model systems in the study of a plethora of phenomena including glass formation, crystallization, sedimentation, clogging and drying of complex mixtures [1–7]. They are also widely used as additives in cosmetics, paints, inks and foods, where they modify the properties of the products [8, 9]. Traditionally, the experimental model of choice for studying the structure and dynamics of glasses or crystals are hard-sphere colloids [3, 10–12], which interact solely through volume exclusion. An analogy with molecular or atomic systems is often drawn, in which each colloidal particle in the suspension represents an atom or molecule. Moreover, recent experiments suggest that making the individual particles deformable allows an even wider range of phenomena to be observed [2, 3, 10, 13, 14]. Deformability can be achieved experimentally by using microgel particles, which are colloidal particles made from a cross-linked and solvent-swollen polymer gel.

A frequently used microgel system is that synthesized from *N*-isopropylacrylamide (NIPAm) and acrylic acid

[4] Present address: Laboratory of Physical Chemistry and Colloid Science, Wageningen University, Dreijenplein 6, 6703 HB Wageningen, The Netherlands.

(AAc), resulting in a copolymer, poly(*N*-isopropylacrylamide) -co-(acrylic acid), or p(NIPAm-co-AAc) [2, 15, 16]. The phase behaviour of suspensions of such pNIPAm-based particles depends strongly on temperature, pH and ionic strength [15, 17–20]. The response of the microgels to such external triggers can be exploited: for instance, size changes induced by a change of temperature can be used to switch between the liquid and crystalline states of the suspension [16, 21–25]. Thermal quenching protocols have also been used to study the physical ageing in microgel glasses [26–29]. The inter-particle potential of p(NIPAm-co-AAc) microgels is also influenced by the pH and ionic strength; at low pH the acrylic acid groups are largely protonated and uncharged, whereas they become more charged due to deprotonation as the pH increases. Added salt can screen these charges and reduce the electrostatic repulsion. An additional effect occurs at low pH; hydrogen bonds can form between protonated carboxylic acid groups and acrylamide moieties of the pNIPAm. This leads to a weak attraction, with a depth of attraction of approximately $0.5k_BT$, as characterized by measurements of the 2D pair correlation function [19]. Observations of concentrated p(NIPAm-co-AAc) suspensions at pH values between 3.0 and 6.0, after a waiting time of several weeks, have shown that pH plays an important role in determining the structure of the final state of these systems; suspensions at low pH age to form crystals over a broad range of concentrations, while at neutral pH they remain fluid-like and form glasses at sufficiently high concentrations [15]. The transitions from an initially fluid state to a final solid-like state have not been studied in detail. It is thus essential to examine how both structure and dynamics evolve during the course of the transitions.

In this paper we investigate in detail how the dynamics and structure of p(NIPAm-co-AAc) suspensions evolve over time after a quench from the liquid state. By directly observing the systems both at low pH, where the particles are weakly attractive, and at neutral pH, where they are purely repulsive, using 3D confocal microscopy we investigate the influence of the inter-particle potential on the temporal evolution of microstructure and the associated changes in single-particle dynamics. At low pH, an initially fluid-like system slows down gradually due to the formation of crystalline structures. Nucleation occurs homogeneously throughout the system and does not appear to be localized at sample boundaries. We show that the freezing transition from the disordered fluid-like state to the solid-like crystalline state is a nucleation-limited process which can take up to a few hours to complete. In contrast, at neutral pH, a fluid-like system retains its disordered structure, characterized by a lack of long-range order, throughout the duration of the experiment. In this case, the dynamics are governed solely by the concentration of the particles and do not depend on the time since the initial quench. We provide detailed information on the evolution of these systems by directly observing the structure of the suspensions and the dynamics of individual particles as a function of time.

2. Materials and methods

Our system consists of poly(*N*-isopropylacrylamide-co-acrylic acid) particles cross-linked with *N*′-*N*′-methylene bisacrylamide synthesized by precipitation polymerization [30–32], yielding microgels with a fully swollen size in the range of 1.0–1.5 μm in diameter as measured by dynamic light scattering in dilute solutions [33]. The particles are fluorescently labelled using PolyFluor 570 (Polysciences Inc.), which copolymerizes with the p(NIPAm-co-AAc) network. After the synthesis, the particles are cleaned by repeated centrifugation and redispersion in deionized water. The resulting suspensions are concentrated by dialysing against a 10 wt% solution of dextran, with a molecular weight of 70 kg mol^{-1}, resulting in an applied osmotic pressure of approximately 20 kPa [34]. A series of suspensions of varying concentrations are prepared by dilution from a concentrated suspension. A few microlitres of sample are then placed in a glass sample cell, which is hermetically sealed to prevent drying or convection.

Images are recorded using a confocal fluorescence microscope (Leica SP5) equipped with a 100× oil immersion objective. As the swollen microgels contain more than 90% solvent, their density and refractive index are very similar to those of the solvent, which respectively minimize the effects of sedimentation and of optical artefacts due to scattering. By optimizing the laser power and the gain on the photomultiplier tubes (PMTs), we can image the same field of view for several hours without significant loss of contrast due to photobleaching. This eliminates the need for an anti-bleaching agent that could alter the chemical environment of the suspension. The 3D field of view for our image stacks is $35 \times 35 \times 10$ μm^3, containing between 5000 and 10 000 particles. Images are recorded at a distance of $\sim$10 particle diameters away from the bottom coverslip and several tens of microns away from the side walls to minimize wall effects.

The centres of the microgel particles appear brighter than their outer parts in the microscopy images; this is due to the fact that microgel particles made by precipitation polymerization are not homogeneous in density, but exhibit a heterogeneous core–shell-type structure [35, 36] with a denser core of cross-linked polymer and a corona, or shell, where the polymer concentration and cross-link density are much lower. The corresponding radial gradient in the dye concentration allows us to identify individual particles even at very high packing densities, as the particle cores remain optically separated. Unfortunately this obscures any direct observation of possible shape deformation of the particles.

As a result of deformability of the microgel particles, their volume changes and the traditional definition of volume fraction in colloidal suspensions no longer reflects the concentration of particles in the systems. We therefore define concentration as $\zeta = V_o n$, where V_o is the volume computed using the hydrodynamic radius and n is the number density of particles [2]. Because a direct measurement of the particle radius is difficult, an accurate determination of the particle volume fraction is not straightforward. In our experiments,

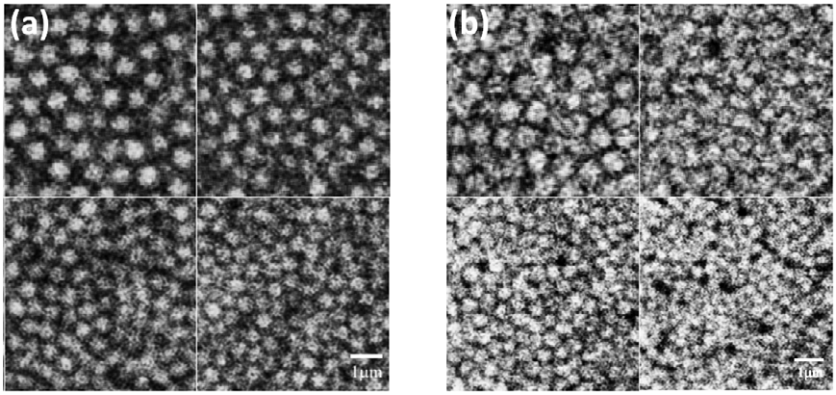

Figure 1. Microgel particles imaged at progressively higher concentrations at pH = 3.3. The particle size decreases systematically and the core shape remains approximately spherical. (a) Particles with cross-linker to monomer ratio of 10% for $\zeta = 0.79$, 1.21, 1.35 and 1.40. (b) Particles with cross-linker to monomer ratio of 4% for $\zeta = 0.61$, 1.1, 2.1 and 3.3, respectively. The highest concentration samples are prepared by dialysis against a dextran solution with an osmotic pressure of ∼20 kPa.

ζ is obtained by counting the number of particles in a 3D image stack. For low volume fraction suspensions, where the particles are highly mobile, an accurate acquisition of a 3D image stack is difficult. For these samples, we count the number of particles in a 2D image, which ranges between 1300 and 2300, and average over several subsequent frames. To measure the number density of particles we define a volume $L \times L \times dz$, where L^2 is the area of the square field of view and dz is the thickness within which the centres of the particles that appear in a 2D image are located. In our case $dz \approx 2a$, where a is the hydrodynamic radius of the particles. To test the accuracy of this 2D estimate for ζ we compare the results obtained in 2D and 3D for an arrested sample, and find a difference in ζ of less than 5%.

We initialize the sample by quenching from a temperature above the lower critical solution temperature (LCST) of pNIPAm to room temperature, where the particles become fully swollen [37]. The sample is then kept at room temperature for 1 h, which is sufficient time for the particles to swell and reach thermal equilibrium [28]. We then collect image sequences, separated in time by an hour, at three different concentrations and for two different pH values (cross-linker to monomer ratio of 8% for $\zeta = 0.6$, 0.65 and 0.71 at pH = 3.3 and $\zeta = 0.75$, 0.80 and 1.18 at pH = 7.0). After image acquisition, the particle positions are determined using particle tracking algorithms [38].

3. Results and discussion

At low volume fractions, microgel particles behave effectively as hard spheres [39]. However, at higher concentrations, the microgels must shrink. This becomes apparent in confocal microscopy images, where we observe a significant reduction of the particle size upon increasing the concentration, as shown in the image series in figures 1(a) and (b) for samples with cross-linker to monomer ratios of 10% and 4%, respectively, at pH = 3.3. The samples with the highest concentration are prepared from dilute suspensions using dialysis against a dextran solution with an osmotic pressure of ∼20 kPa; the lower concentration samples are obtained by dilution of these concentrated samples. The significant difference in softness between these samples becomes apparent already during sample preparation, as particles with a cross-linker to monomer ratio of 4% shrink more than those with a ratio of 10% even though the same osmotic pressure is applied. This difference is evident when comparing the most concentrated samples in figures 1(a) and (b). A similar trend in size change of particles with concentration is seen in all our other samples for a range of cross-linker to monomer ratios. Such deswelling of microgels is also observed in other situations; for example, when a large and soft microgel is introduced into a crystalline array of smaller and stiffer particles, the large microgel can shrink to conform to the crystal lattice [40].

To quantify this deswelling of particles and the corresponding suspension structures, we track the positions of microgel particles in the confocal images and calculate the 3D radial pair correlation function, $g(r)$, which reflects the probability of finding a particle at a distance r from the centre of any arbitrary reference particle [41]. The position of the first peak in the pair correlation function corresponds to the average distance to the nearest neighbour. We find that the position of the first peak, r_1, decreases with increasing number density n as shown in figure 2. For isotropic deswelling r_1 should decrease as $n^{-1/3}$. Our observations are consistent with this expected scaling as illustrated by the solid line of slope $-1/3$ in figure 2 for the sample with a cross-linker to monomer ratio of 4% at pH = 3.3 and 7.0. At high pH, the number density is lower since the particles are bigger.

Our microgel particles exhibit a soft repulsive interaction potential; by changing the pH from neutral to acidic, an additional attractive interaction between the particles is introduced [19]. Here we make use of this tunability to investigate the effects of the inter-particle potential on the dynamics and structure of these suspensions. The system follows distinct routes to dynamic arrest: at low pH, attraction-driven crystallization dominates the evolution in the dynamics, while at neutral pH the evolution is dictated by concentration. The dynamics can be quantified by computing the mean square displacement (MSD), $\langle \Delta x^2(t) \rangle$, of the

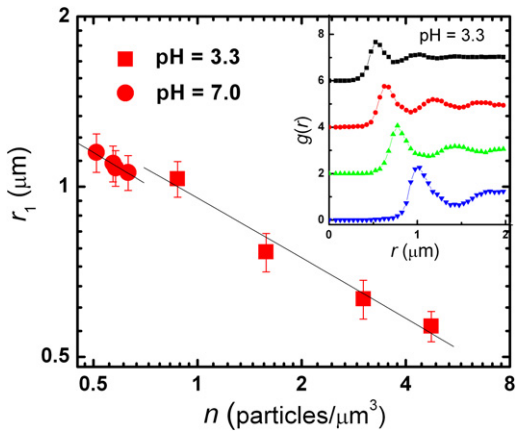

Figure 2. First peak position of $g(r)$ plotted as a function of number density, n, for the sample with cross-linker to monomer ratio of 4% at pH = 3.3 and 7.0. The solid line shows a power law with exponent $-1/3$ for comparison. Inset: radial pair correlation functions, $g(r)$, for the sample at pH = 3.3; curves are offset in increments of 2 for clarity.

particles from image sequences acquired at the two different pH levels. For the attractive suspension, at short lag times, the MSD increases linearly in time, thus indicating a diffusive behaviour. At increasing lag time, the sample reaches an arrested state where the MSD exhibits a plateau due to crystallization, as shown in figure 3(a) for a sample at pH = 3.3 and $\zeta = 0.65$. In contrast, for the purely repulsive systems the MSD exhibits almost no temporal evolution, as shown in figure 3(b) for a sample at pH = 7.0 and $\zeta = 0.75$. The dynamics remain purely diffusive, even after a waiting time of up to 12 h after quenching from the fluid state. Clearly, the two systems exhibit qualitatively different behaviour.

This behaviour can be quantified by extracting the slope α of the MSD: $\langle \Delta x^2(t) \rangle \propto t^{\alpha}$, where $0 \leq \alpha \leq 1$. For diffusion, the exponent is equal to unity, giving $\langle \Delta x^2 \rangle = 2D^*t$, where D is the diffusion constant [42]. The behaviour for which $\alpha < 1$ is known as sub-diffusive; while for a fully arrested system, $\alpha = 0$. At $\zeta = 0.60$ and low pH, the sample remains diffusive during the entire experiment. For a slightly higher concentration of $\zeta = 0.65$ of attractive particles, the mean square displacements reveal that the sample slowly evolves from a liquid-like state, characterized by a diffusive mobility of the microgels ($\alpha = 1$) to a fully arrested state ($\alpha = 0$), after approximately 12 h. At an even higher concentration, $\zeta = 0.71$, diffusivity of particles is restricted, even directly after quenching, as can be concluded from a smaller value of $\alpha = 0.5$; moreover the dynamics become even slower with time. This sequence of events is represented in the plot as a function of time for different ζ (figure 3(c)). At high concentration and low pH, where movement of the particles is highly constrained immediately upon quenching, no relaxation is observed and a glassy system results. In contrast, the purely repulsive systems, at neutral pH, and at $\zeta = 0.75$ and 0.8 remain fluid-like over the entire course of the experiment, with the latter displaying slower dynamics. Reinspection of the neutral pH sample at $\zeta = 0.75$ after six days still shows a

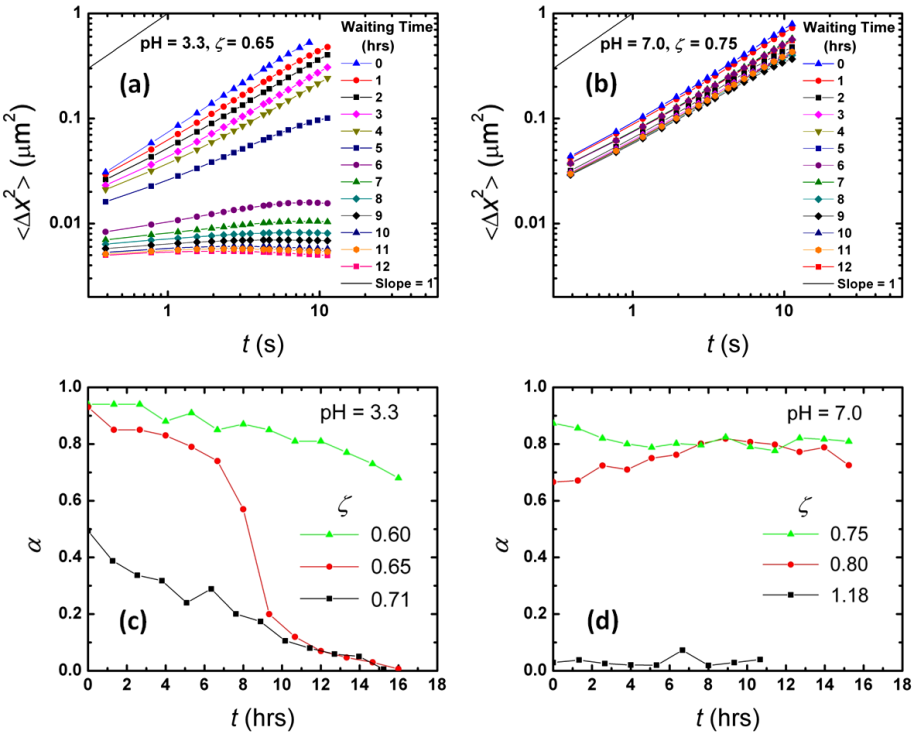

Figure 3. The x component of mean square displacements of 2D image sequences for samples at two different pH levels for successive waiting times in h. (a) pH = 3.3 and $\zeta = 0.65$, (b) pH = 7.0 and $\zeta = 0.75$. (c) α, the slope of the MSD curves in (a) as a function of waiting time at pH = 3.3 for $\zeta = 0.6$, 0.65 and 0.71. (d) α at pH = 7.0 for $\zeta = 0.75$, 0.80 and 1.18.

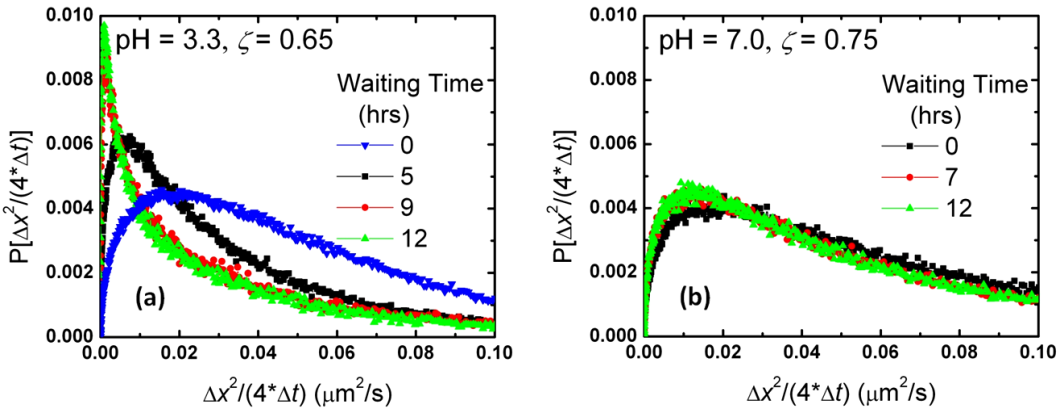

Figure 4. Probability distributions of particle mobilities as a function of waiting time. The plots are normalized such that the areas under the curves are equal to 1. (a) pH = 3.3, $\zeta = 0.65$, $\Delta t = 1.56$ s and (b) pH = 7.0, $\zeta = 0.75$, $\Delta t = 1.56$ s.

completely fluid-like state. At higher particle concentrations ($\zeta = 1.18$), where particles are hindered by crowding and are purely repulsive, a disordered arrested state with $\alpha = 0$ is observed and these samples do not show any signs of change in their dynamics, such as ageing, over the course of the experiment (figure 3(d)). While the dynamics of the attractive suspensions strongly evolves over time for a given concentration, the dynamics of the purely repulsive samples stay unchanged and depend on particle concentration only.

A more detailed view on how these samples evolve is obtained from the probability, $P(D_s)$, of finding a certain mobility $D_s = \Delta x^2/(4^*\Delta t)$, calculated for a fixed time interval $\Delta t = 1.56$ s. For a diffusive system of monodisperse colloids, the probability distribution should display a Gaussian shape centred on the diffusion coefficient of the particles. The attractive microgels show a strong decrease in mobility over time; the peak position shifts by more than a decade in 12 h, as shown in figure 4(a). The distribution is very broad with a strong non-Gaussian behaviour at the start and becomes sharper with time; this suggests that dynamical heterogeneities that cause the distribution to broaden and deviate from a Gaussian shape are gradually becoming less prevalent. The reason for this behaviour can be found in the confocal images; the initially fluid-like sample begins to crystallize, starting with small domains of crystals, which grow until the crystal spans the entire field of view. Due to the different dynamics in the crystalline and fluid regions of the suspension, the coexistence of these two phases leads to a pronounced heterogeneity in the dynamics. The dynamical heterogeneity thus decreases again as crystallization spreads across the sample.

The purely repulsive samples show a qualitatively different behaviour; no changes in the distribution of mobilities are observed over the course of the experiment, as shown in figure 4(b). There are, however, significant deviations from a Gaussian distribution in the sample close to the glass transition; such strong dynamical heterogeneity in the absence of structural heterogeneity is one of the characteristic features of colloidal suspensions approaching the glassy state [10, 43]. Although rheological experiments have indicated that suspensions of microgel particles show pronounced ageing of the rheological properties of the suspension after a quench into the glassy state [27, 29] we found no evidence of ageing for the sample shown in figure 4(b) with $\zeta = 0.75$.

These differences between the low pH and neutral pH samples are also apparent from comparing the structures in the initial and final states of the suspensions directly from confocal images, as shown in figure 5. In the attractive systems, at low pH, crystalline domains nucleate from a fluid-like configuration; these domains grow rapidly until the entire sample reaches an ordered state. These initial and final states are shown in figures 5(a) and (b) for the sample at $\zeta = 0.65$. In contrast, for the purely repulsive systems, no signs of order or significant structural evolution are observed. The initial disordered state is maintained, both at lower densities where the particles are mobile, as well as at higher densities where the sample exhibits glass-like behaviour, as shown in figures 5(c) and (d) for a sample with purely repulsive particles at $\zeta = 0.75$ both directly after the quench and after approximately 12 h.

To quantify the growth of crystal domains after nucleation, we investigate a time series of 2D images taken parallel to the bottom coverslip and identify fluid-like and crystal-like regions on each image by eye. An example of such an image sequence of *xy* images is shown in figures 6(a)–(d) for pH = 3.3 and $\zeta = 0.65$, where we have marked the fluid regions by inverting the image. For attractive samples at low pH we generally observe nucleation of crystalline domains throughout the sample and subsequent growth of these domains until they span the entire field of view. Crystal dynamics is characterized by an almost instantaneous increase of crystallinity of the suspension in a fashion that is reminiscent of the nucleation-limited crystallization of hard-sphere colloids [44, 45]; after the time-limiting nucleation step has occurred, growth of the crystal nuclei is almost instantaneous. This is supported by other findings on crystallization of microgel particles where an increase of the degree of crystallinity was observed on a timescale of several minutes [25].

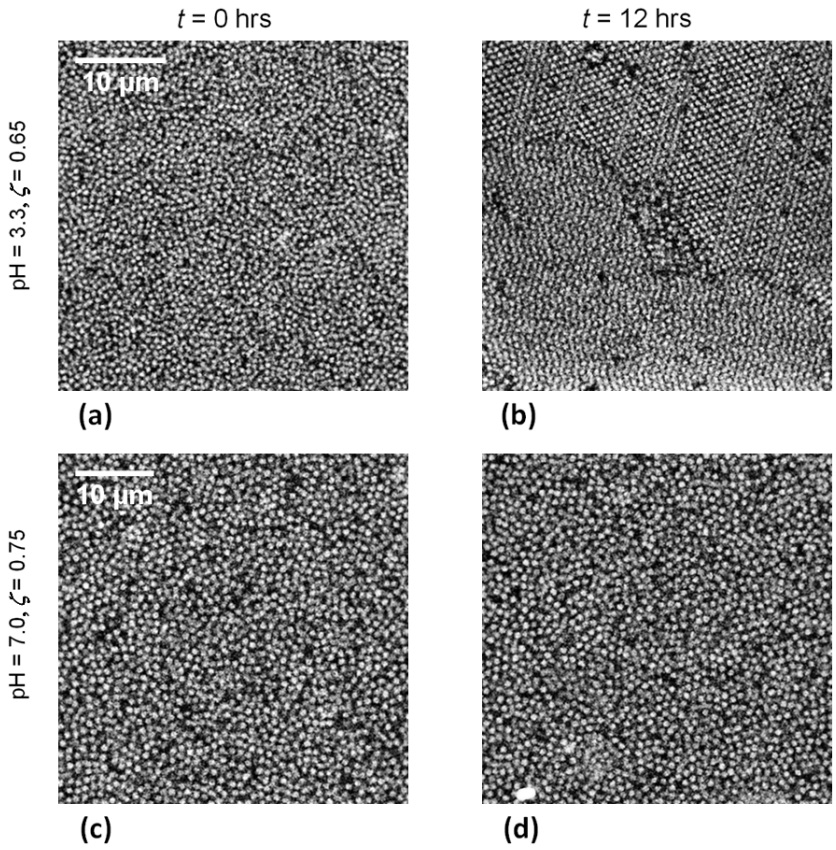

Figure 5. ((a), (b)) Development of structure at pH 3.3 and $\zeta = 0.65$ for waiting times $t = 0$ h and $t = 12$ h, respectively. After 12 h the sample is dynamically arrested forming crystalline domains. ((c), (d)) Development of structure at pH $= 7.0$ and $\zeta = 0.75$ for waiting times $t = 0$ and 12 h.

To further investigate the crystallization process, we follow the microgel behaviour during crystallization within the *xz* plane, the cross section perpendicular to the bottom coverslip. Figure 6(e) shows the same sample as the one shown in figures 6(a)–(d) imaged in the *xz* plane. The lines mark the crystal domains that nucleated and grew separately. At later times, such domains form throughout the sample. The growth of crystal domains thus appears to occur isotropically, until different grain boundaries meet. The crystal domains nucleate in the bulk of the sample and not at the coverslip; this suggests that nucleation of crystals at the walls of the sample cell does not play an important role.

A more complete sequence of images similar to figures 6(a)–(d) is used to obtain figure 6(f), where we have plotted the area fraction of ordered particles as a function of waiting time for samples at pH $= 3.3$ and a cross-linker to monomer ratio of 8% at $\zeta = 0.65$, 0.68 and 0.71 (●), 1% at $\zeta = 0.79$ (■) and 10% at $\zeta = 0.63$ (▲). The lag time between initialization of the sample and the fast growth of crystals depends strongly on ζ; the higher the packing density the faster nucleation occurs. From our data it also appears that the softness of the particles influences the nucleation rate; soft particles, with a cross-linker to monomer ratio of 1%, crystallize slower than stiffer particles, with 8% cross-linker to monomer ratio. Moreover, we note that, due to the relatively large typical size of the crystalline regions compared to the size of the field of view, our manual method for determining the fraction of crystalline regions may not be representative for the entire sample. Nevertheless, this method yields surprisingly repeatable results and we find that the determined crystallization kinetics remain qualitatively similar across the different concentrations and particle softnesses explored here. This indicates that our manual procedure for estimating the fraction of crystalline regions is surprisingly accurate.

To further quantify the evolution of these samples towards their crystalline state, we also study the microgel dynamics. While the microgel particles are diffusive in the fluid, they become kinetically arrested in the crystalline state. Information about the crystallization process can thus also be obtained by analysing the mean square displacement of individual particles. Here we define particles that have a mean square displacement less than 0.1 μm^2, after a lag time of 400 ms, as kinetically arrested, while particles that are well into the fluid regime display a typical mean square displacement of 0.6 μm^2 after the same lag time. If we reconstruct our sample by colour-coding slow particles in yellow and fast particles in blue, we can clearly follow the evolution from an initially fluid state to a final, fully crystalline solid, as shown in figures 7(a)–(d). Comparison of this image sequence with the confocal time sequence in figures 6(a)–(d) qualitatively confirm the particle dynamics indeed evolve in a similar fashion as does the ordering of particles into crystalline domains. The fraction of 'slow' particles, which take part in crystalline domains, show

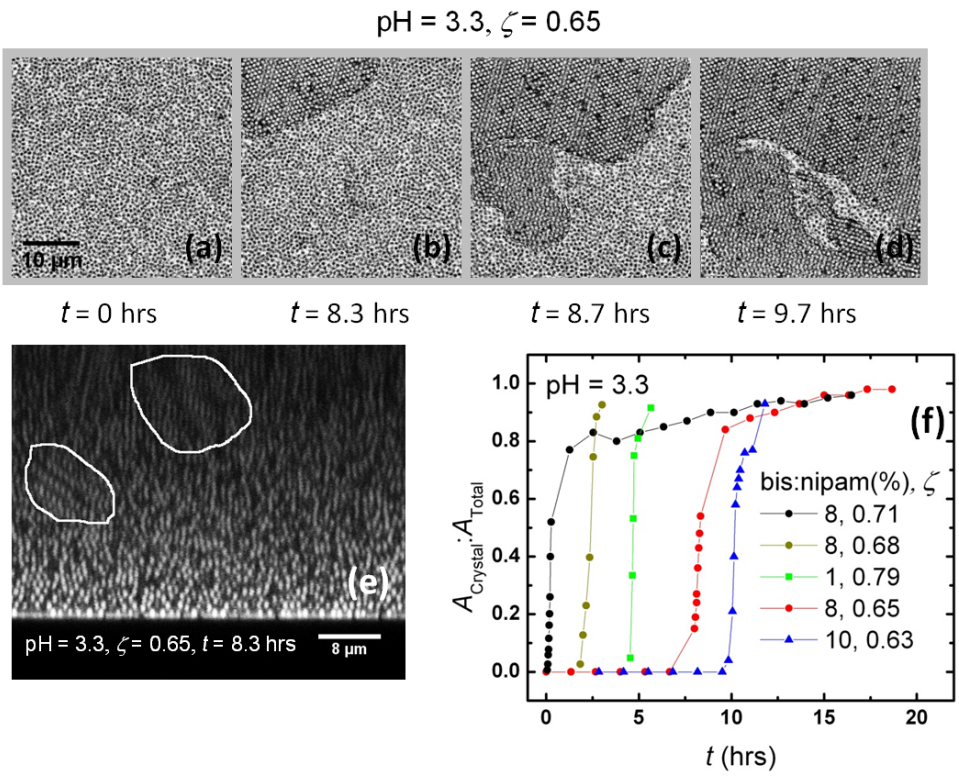

Figure 6. Crystallization kinetics of microgel particles at pH = 3.3. (a)–(d) Images taken parallel to the bottom coverslip of a sample at pH = 3.3 and $\zeta = 0.65$. Non-crystalline areas are highlighted by inverting the image. (e) An image taken perpendicular to the coverslip of a sample at pH = 3.3, $\zeta = 0.65$ and waiting time 8.3 h. (f) The area fraction of ordered particles as a function of time for cross-linker to monomer ratio of 8% at $\zeta = 0.71$, 0.68 and 0.65 from left to right (●), 1% at $\zeta = 0.79$ (■), and 10% at $\zeta = 0.63$ (▲).

dynamics very similar to those obtained from the 2D area fractions shown in figure 6(f). The fraction of microgels that are in a crystalline region is initially close to zero, until nucleation takes place, where it suddenly and steeply increases until almost all of the particles participate in ordered domains. Analysing the crystallization kinetics based on this dynamic criterion gives, within experimental error, the same result as that found by direct inspection of the 2D confocal images. This is demonstrated by the correspondence between the two metrics in figure 7(e) for a sample with a cross-linker to monomer ratio of 8% at pH = 3.3 and $\zeta = 0.65$, 0.68. In contrast, the reconstruction at high pH and high concentration does not display structural or dynamical evolution over time as shown in figures 7(f)–(h) for the sample at pH = 7.0 and $\zeta = 1.18$.

The temporal evolution of the suspension structure can be further observed by plotting the pair correlation functions. We plot $g(r)$ in figure 8(a) to elucidate this evolution as a function of time. For the attractive particles, $g(r)$ depends strongly on the age of the sample, changing continuously from a behaviour typical for a fluid, without any long-range order, to a $g(r)$ that exhibits hallmarks of crystalline structure, with well-defined peaks that extend to many particle diameters, indicating the presence of relatively long-ranged order in the sample. In contrast, for the purely repulsive system, the $g(r)$ does not evolve over time and remains fluid-like with an absence of any long-range order (figure 8(b)).

At low volume fractions, microgel suspensions with purely repulsive inter-particle potentials behave similar to hard spheres [39]. It is thus appealing to attempt to map the dynamics and phase behaviour of microgel particles onto the well-understood behaviour of suspensions of hard-sphere colloids. One approach is to use the Percus–Yevick (PY) closure approximation [46, 47] for hard spheres to predict the pair correlation function for a fluid-like microgel system by using an effective hard-sphere volume fraction. Indeed, the $g(r)$ for the purely repulsive microgel system can be well described by a PY structure factor, as shown in figure 8(b). We used the radius derived directly from the confocal microscopy images as the effective radius; this value also corresponds to the location of the first peak in $g(r)$. The $g(r)$ was then fitted with a PY expression to obtain an effective hard-sphere volume fraction $\phi_{\text{eff}} = 0.47$. This is significantly lower than the value of $\zeta = 0.8$, which was computed using the measured particle diameter in the dilute state. This indicates that, even though our particles are soft, their structural order is similar to that of particles interacting via a hard-sphere potential.

We thus find that microgels follow distinct routes towards dynamic arrest that depend sensitively on the pH of the suspensions. In following these routes, we find that slightly attractive microgels have a strong tendency to crystallize even at very low concentrations; nucleation of crystals occurs homogeneously throughout the sample. Once nucleation takes place, we observe a rapid growth of crystals on a timescale of several minutes and a subsequent kinetic arrest of the

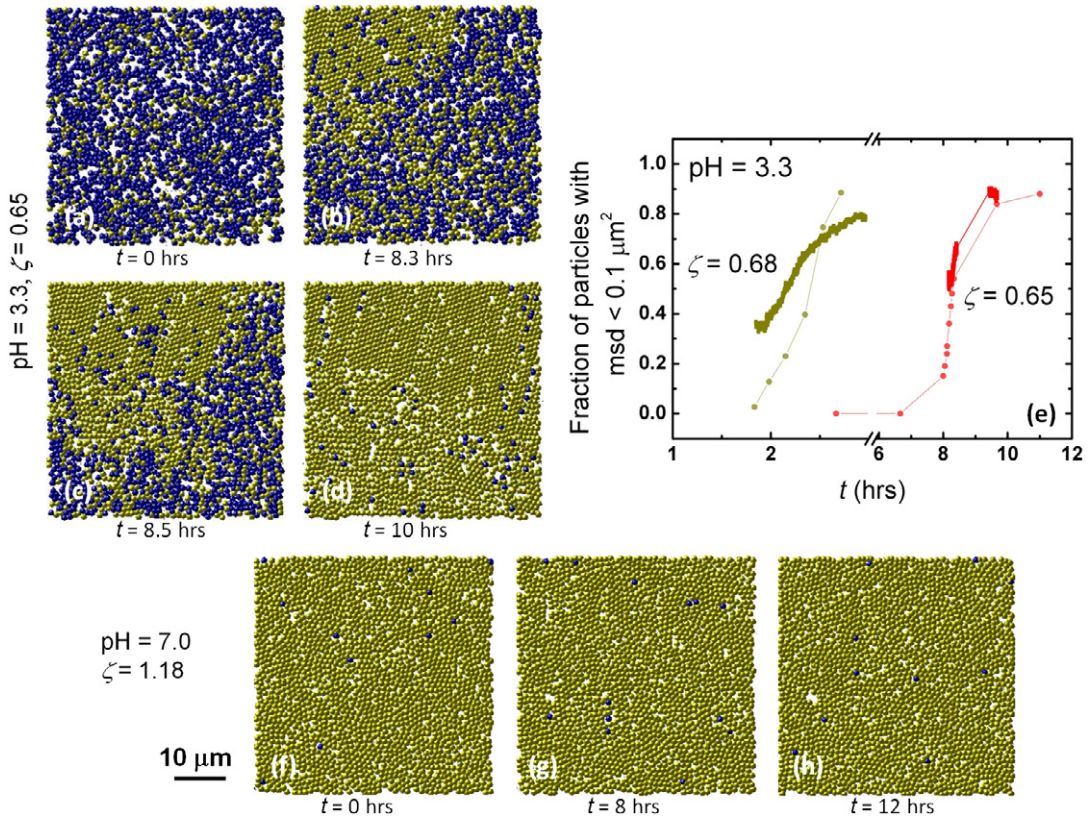

Figure 7. Particles colour-coded according to their MSD for cross-linker to monomer ratio of 8%. Yellow coded particles have MSD < 0.1, while blue coded particles have MSD > 0.1. (a)–(d) pH $= 3.3$, $\zeta = 0.65$. Waiting times are (a) 0 h, (b) 8.3 h, (c) 8.5 h and (d) 10 h. (e) Number fraction of slow particles with MSD $< 0.1\ \mu m^2$ plotted as a function of time for cross-linker to monomer ratio of 8% at $\zeta = 0.68$ and 0.65 (■). Corresponding area fractions of ordered particles from figure 6(f) are included for comparison (●). (f)–(h) pH $= 7.0$, $\zeta = 1.18$. Waiting times are (f) 0 h, (g) 8 h and (h) 12 h.

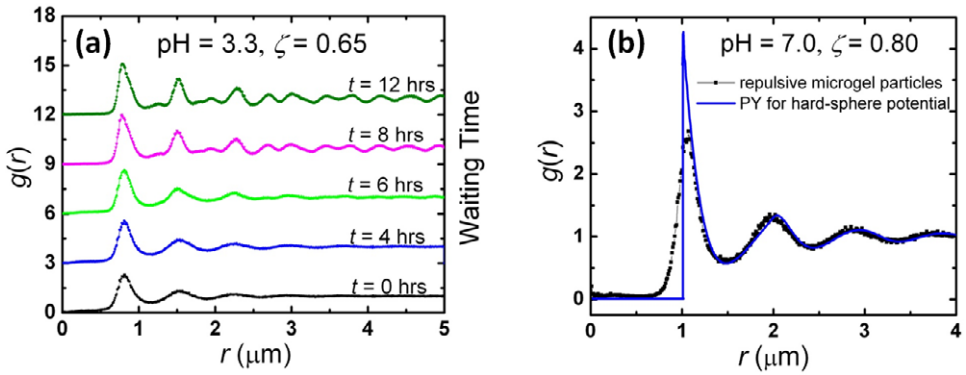

Figure 8. Structural evolution. (a) Pair correlation functions for $\zeta = 0.65$ at pH $= 3.3$ as a function of waiting time. (b) Pair correlation function measured for a sample of repulsive microgels for $\zeta = 0.80$ at pH $= 7.0$. Percus–Yevick approximation for the pair correlation function (solid line) is included.

system. Concentration also plays a role during kinetic arrest. For the low pH samples at high concentrations, relaxation is restricted and the system arrests forming a disordered solid, whereas they crystallize at low concentrations. In contrast, at high pH, the dynamics are solely a function of the microgel concentration and at low concentration, the suspension stays fluid-like for the entire period of the experiment and no kinetic arrest is observed; here, crystallization is possible within a range of concentrations, $\zeta \sim 0.5$–1.0, only. At higher concentrations, the system forms a glassy state.

4. Conclusion

The interaction between microgel particles of p(NIPAm-co-AAc) can be tuned from purely repulsive to also include an attractive component by changing the pH. In this study we

use confocal microscopy to explore the effects of changes in interaction potential on the development of the structure and dynamics of microgel systems. Our results illustrate that systems with and without an attractive contribution to the inter-particle potential develop in quantitatively different manners. The attractive systems crystallize to form a solid even at low microgel particle concentrations. Crystallization in the microgel system is nucleation-limited, where there is a sudden and fast rise in crystallinity upon the formation of nuclei, which occurs after a delay time. In addition, nucleation appears to happen homogeneously throughout the sample and not preferentially close to the sample boundaries. In contrast, for microgel suspensions without an attractive interaction, the behaviour of the system is only a function of particle concentration. Our results thus illustrate that small changes in the interaction potential can have a dramatic effect on the temporal evolution of the dynamics and structure in suspensions of deformable colloids.

Acknowledgments

JS thanks the Netherlands Organization for Scientific Research (NWO) for financial support. We thank Eric Weeks and John Crocker for use of their particle tracking algorithms. This work was supported by the Harvard MRSEC (DMR-0820484), and the NSF (DMR-1006546).

References

[1] Xu L, Davies S, Schofield A B and Weitz D A 2008 Dynamics of drying in 3d porous media *Phys. Rev. Lett.* **101** 094502
[2] Mattsson J, Wyss H M, Fernandez-Nieves A, Miyazaki K, Hu Z, Reichman D R and Weitz D A 2009 Soft colloids make strong glasses *Nature* **462** 83–6
[3] Megen W van and Pusey P N 1991 Dynamic light-scattering study of the glass transition in a colloidal suspension *Phys. Rev.* A **43** 5429–41
[4] Schall P, Cohen I, Weitz D A and Spaepen F 2004 Visualization of dislocation dynamics in colloidal crystals *Science* **305** 1944–8
[5] Allain C, Cloitre M and Wafra M 1995 Aggregation and sedimentation in colloidal suspensions *Phys. Rev. Lett.* **74** 1478–81
[6] McDowell-Boyer L M, Hunt J R and Sitar N 1986 Particle transport through porous media *Water Resour. Res.* **22** 1901–21
[7] Wyss H M, Blair D L, Morris J F, Stone H A and Weitz D A 2006 Mechanism for clogging of microchannels *Phys. Rev.* E **74** 061402
[8] Bradna P, Stern P, Quadrat O and Snuparek J 1995 Thickening effect of dispersions of ethyl acrylate-metacrylic acid copolymer prepared by different polymerization routes *Colloid Polym. Sci.* **273** 324–30
[9] Das M, Zhang H and Kumacheva E 2006 Microgels: old materials with new applications *Annu. Rev. Mater. Res.* **36** 117–42
[10] Weeks E R, Crocker J C, Levitt A C, Schofield A and Weitz D A 2000 Three-dimensional direct imaging of structural relaxation near the colloidal glass transition *Science* **287** 627–31
[11] Pusey P N and Megen W v 1987 Observation of a glass transition in suspensions of spherical colloidal particles *Phys. Rev. Lett.* **59** 2083–6
[12] Megen W van and Underwood S M 1994 Glass transition in colloidal hard spheres: measurement and mode-coupling-theory analysis of the coherent intermediate scattering function *Phys. Rev.* E **49** 4206–20
[13] Jackle J 1986 Models of the glass transition *Rep. Prog. Phys.* **49** 171–231
[14] Angell C A, Ngai K L, McKenna G B, McMillan P F and Martin S W 2000 Relaxation in glassforming liquids and amorphous solids *J. Appl. Phys.* **88** 3113–57
[15] Meng Z, Cho J K, Breedveld V and Lyon L A 2009 Physical aging and phase behavior of multiresponsive microgel colloidal dispersions *J. Phys. Chem.* B **113** 4590–9
[16] Lyon L A, Debord J D, Debord S B, Jones C D, McGrath J G and Serpe M J 2004 Microgel colloidal crystals *J. Phys. Chem.* B **108** 19099–108
[17] Wu J, Zhou B and Hu Z 2003 Phase behavior of thermally responsive microgel colloids *Phys. Rev. Lett.* **90** 048304
[18] John A N S, Breedveld V and Lyon L A 2007 Phase behavior in highly concentrated assemblies of microgels with soft repulsive interaction potentials *J. Phys. Chem.* B **111** 7796–801
[19] Cho J K, Meng Z, Lyon L A and Breedveld V 2009 Tunable attractive and repulsive interactions between ph-responsive microgels *Soft Matter* **5** 3599–602
[20] Gottwald D, Likos C N, Kahl G and Lowen H 2004 Phase behavior of ionic microgels *Phys. Rev. Lett.* **92** 068301
[21] Han Y, Ha N Y, Alsayed A M and Yodh A G 2008 Melting of two-dimensional tunable-diameter colloidal crystals *Phys. Rev.* E **77** 041406
[22] Zhang Z, Xu N, Chen D T N, Yunker P, Alsayed A M, Aptowicz K B, Habdas P, Liu A J, Nagel S R and Yodh A G 2009 Thermal vestige of the zero-temperature jamming transition *Nature* **459** 230–3
[23] Meng Z, Cho J K, Debord S, Breedveld V and Lyon L A 2007 Crystallization behaviour of soft, attractive microgels *J. Phys. Chem.* B **111** 6992–7
[24] Hellweg T, Dewhurst C D, Bruckner E, Kratz K and Eimer W 2000 Colloidal crystals made of poly(n-isopropylcrylamide) microgel particles *Colloid Polym. Sci.* **278** 972–8
[25] Tang S, Hu Z, Cheng Z and Wu J 2004 Crystallization kinetics of thermosensitive colloids probed by transmission spectroscopy *Langmuir* **20** 8858–64
[26] Erwin B M, Vlassopoulos D and Cloitre M 2010 Rheological fingerprinting of an aging soft colloidal glass *J. Rheol.* **54** 915–39
[27] Cloitre M, Borrega R and Leibler L 2000 Rheological aging and rejuvenation in microgel pastes *Phys. Rev. Lett.* **85** 4819–22
[28] Yunker P, Zhang Z, Aptowicz K B and Yodh A G 2009 Irreversible rearrangements, correlated domains, and local structure in aging glasses *Phys. Rev. Lett.* **103** 115701
[29] Purnomo E H, Ende D v d, Vanapalli S A and Mugele F 2008 Glass transition and aging in dense suspension of thermosensitive microgel particles *Phys. Rev. Lett.* **101** 238301
[30] Wu X, Pelton R H, Hamielec A E, Woods D R and McPhee W 1994 The kinetics of poly(*N*-isopropylacrylamide) microgel latex formation *Colloid Polym. Sci.* **272** 467–77
[31] Duracher D, Elaissari A and Pichot C 1999 Preparation of poly(n-isopropylmethacrylamide) latexes kinetic studies and characterization *J. Polym. Sci.* A **37** 1823–37
[32] Pelton R 2000 Temperature-sensitive aqueous microgels *Adv. Colloid Interface Sci.* **85** 1–33
[33] Dhont J K G 1996 *An Introcution to Dynamics of Colloids* (Amsterdam: Elsevier) pp 107–70
[34] Livney Y D, Ramon O, Kesselman E, Cogan U, Mizrahi S and Cohen Y 2001 Swelling of dextran gel and osmotic

pressure of soluble dextran in the presence of salts *J. Polym. Sci.* B **39** 2740–50
[35] Mason T G and Lin M Y 2005 Density profiles of temperature-sensitive microgel particles *Phys. Rev.* E **71** 040801
[36] Stieger M, Richtering W, Pedersen J S and Linder P 2004 Small-angle neutron scattering study of structural changes in temperature sensitive microgel colloids *J. Chem. Phys.* **120** 6197–206
[37] Colin R, Alsayed A M, Castaing J-C, Goyal R, Hough L and Abou B 2011 Spacially heterogeneous dynamics in a thermosensitive soft suspension before and after the glass transition *Soft Matter* **7** 4504–14
[38] Crocker J C and Grier D G 1996 Methods of digital video microscopy for colloidal studies *J. Colloid Interface Sci.* **179** 298–310
[39] Senff H and Richtering W 2000 Influence of corss-link density on rheological properties of temperature-sensitive microgel suspensions *Colloid Polym. Sci.* **278** 830–40
[40] Iyer A S J and Lyon L A 2009 Self-healing colloidal crystals *Angew. Chem. Int. Edn* **48** 4562–6
[41] Chaikin P M and Lubensky T C 1997 *Principles of Condensed Matter Physics* (Cambridge: Cambridge University Press) pp 29–42
[42] Einstein A 1905 *Ann. Phys.* **17** 549–60
[43] Sessoms D A, Bischofberger I, Cipelletti L and Trappe V 2009 Multiple dynamic regimes in concentrated microgel systems *Phil. Trans. R. Soc.* A **367** 5013–32
[44] Schope H J, Bryant G and Megen W v 2006 Two-step crystallization kinetics in colloidal hard-sphere systems *Phys. Rev. Lett.* **96** 175701
[45] Harland J L and Megen W V 1997 Crystallization kinetics of suspensions of hard colloidal spheres *Phys. Rev.* E **55** 3054–67
[46] Percus J K and Yevick G J 1958 Analysis of classical statistical mechanics by means of collective coordinates *Phys. Rev.* **110** 1–13
[47] Thiele E 1963 Equation of state for hard spheres *J. Chem. Phys.* **39** 474–9